ACS Catalysis

Research Article

pubs.acs.org/acscatalysis

One-Pot Synthesis of Supported, Nanocrystalline Nickel Manganese Oxide for Dry Reforming of Methane

Xiao Xie,[∥,†] Torsten Otremba,[∥,‡] Patrick Littlewood,[‡] Reinhard Schomäcker,*[,‡] and Arne Thomas*[,†]

[†]Functional Materials and [‡]Reaction Engineering, Department of Chemistry, Technische Universität Berlin, Hardenbergstrasse 40, Berlin 10623, Germany

Supporting Information

ABSTRACT: Silica supported nanoparticles of nickel manganese oxide, $Ni_{0.2}Mn_{0.8}O$, were prepared in a one-pot approach, combining co-precipitation and sol−gel chemistry. This approach enables the preparation of small ternary oxide crystallites evenly dispersed on porous silica. The resulting materials were used as catalyst for dry reforming of methane (DRM), and show a much higher activity as the reference bulk material prepared from conventional co-precipitation. Notably, the catalyst shows a remarkable activity even at low temperatures for DRM, thus nearly reaching thermodynamic equilibrium at 500 °C.

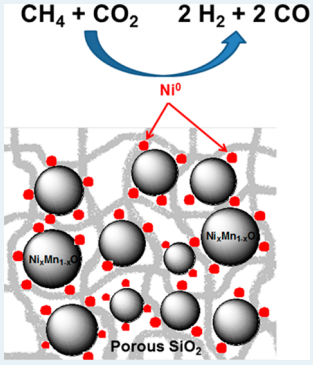

KEYWORDS: *dry reforming, methane, carbon dioxide, activation, heterogeneous catalysis, metal oxide catalyst*

INTRODUCTION

Synthesis gas is an important raw material for several industrial processes, such as methanol synthesis, oxo-synthesis, and Fischer−Tropsch-synthesis. Presently, synthesis gas is mainly generated via partial oxidation of coal, leading to carbon monoxide. In a subsequent process, hydrogen is formed by water-gas-shift-equilibrium from carbon monoxide and water. An alternative route to obtain synthesis gas is CO_2 reforming of methane (DRM). Carbon dioxide and methane are both green house-gases and are available in large amounts which make them interesting reactants for the production of synthesis gas. Moreover, this route could be applied in addition to existing partial oxidation of methane in which carbon dioxide is produced as side product, like the oxidative coupling of methane (OCM). The heat produced by such exothermic oxidation reactions could be conveniently used for providing the energy for the endothermic DRM. Considering the energy loss caused by the heat transfer between reactors where these two separate processes are conducted, it is of course highly desirable to operate the DRM reaction at temperatures 50−100 K below the OCM reaction. However, because of the thermodynamic limitation of the DRM reaction (equilibrium constant 1 at 642 °C with equimolar CH_4 and CO_2) and the poor activity of most catalysts at lower reaction temperature, most of catalysts were investigated in the DRM reaction above 600 °C.[1,2]

Various catalysts have been investigated for DRM, including perovskite type-oxides like $LaNi_{1-x}Ru_xO_3$,[3] $NdCoO_3$,[4] and $La_{2-x}Sr_xNiO_4$,[5,6] supported metal catalysts, often nickel on different supports[7−10] or some other mono- or bimetallic catalysts.[11−16] Moreover, NiO-MgO solid solutions have been recognized as suitable catalysts for the DRM reaction.[17−21] Nickel based catalysts have the advantage that they have shown to be very active even at low temperatures, that is, between 400 and 550 °C.[22−25] For example Ni supported on MgO with 0.1% Pt doping gives 38% conversion of CH_4 at 550 °C which is close to the equilibrium with 45% X_{CH4}.[22,23] Ni supported on mesoporous La_2O_3−ZrO_2 even showed activity at 400 °C.[24]

When the DRM reaction has to be operated at relative low reaction temperatures carbon deposition is a critical issue as this reaction is thermodynamically favored at these conditions. Ni-containing, ternary metal oxides forming solid solutions have proven to be suitable catalysts in this temperature regime. It was suggested that reduced Ni^0 is the active site in the DRM reaction and that in case of solid solution catalysts both oxides are stabilized thus inhibiting formation of large clusters of Ni^0 which causes coke deposition.[20,21,26−28] In this work solid solutions of nickel manganese oxide are tested as catalysts for DRM. Such solid solutions of NiO-MnO can be easily formed under reductive atmosphere.[29] For the preparation of ternary oxides, co-precipitation (cp) is one of the most often applied methods. The respective metal salts are dissolved and then precipitated concurrently to form a solid precursor, which is then transformed into the desired metal oxides by thermal treatment.

For catalytic applications it is generally beneficial to prepare smaller particles to increase the overall surface area of the catalyst and furthermore to disperse them on a porous support

Received: June 19, 2012
Revised: December 21, 2012
Published: December 26, 2012

to prevent agglomeration. Recently supported metal catalysts produced in a one-pot procedure, that is, by directly adding preformed metal nanoparticles to a silica precursor-organic template solution has been reported.[30−33] During the gelation of silica, the nanoparticles were homogeneously distributed within the porous silica phase.

Motivated by this approach we report here a modified one-pot strategy, combining co-precipitation with a sol−gel process. In contrast to the conventional co-precipitation procedure, the metal salt solutions are added to an aqueous solution of sodium silicate, Na_2SiO_3. Under basic conditions, the metals are precipitated concurrently to the gelation of the silica precursor, forming a precursor gel which after heat treatment transforms into dispersed metal oxide nanoparticles on porous SiO_2. The so prepared material is remarkably active (the reaction achieve thermodynamic equilibrium under mild conditions) in comparison to a nonsupported metal oxide as catalyst for the DRM reaction even at low reaction temperature between 500 and 550 °C.

EXPERIMENTAL SECTION

Synthesis of the Catalysts. In this study two ternary metal oxide catalysts, $Ni_{0.2}Mn_{0.8}O\_cp$ and $Ni_{0.2}Mn_{0.8}O\_cp\text{-}SiO_2$ were prepared and tested for the DRM reaction. $Ni_{0.2}Mn_{0.8}O\_cp$ was prepared by a co-precipitation method according to the following procedure: 5 mmol $Ni(OAc)_2{\cdot}4H_2O$ and 20 mmol $Mn(NO_3)_2{\cdot}4H_2O$ were dissolved in 100 mL of deionized water. 30 mmol of $NaHCO_3$ and 20 mg of NaOH dissolved in 50 mL of deionized water were added into the metal precursor solution dropwise under vigorous stirring. The mixture was stirred at room temperature for 6 h, followed by filtration of the precipitate and washing with deionized water. The obtained solid was dried in vacuum at 80 °C overnight and then calcined at 500 °C for 4 h. Quantitative yield was observed. $Ni_{0.2}Mn_{0.8}O\_cp\text{-}SiO_2$ was prepared by a combined co-precipitation/gelation method: 25 mmol $Na_2SiO_3{\cdot}5H_2O$ was dissolved in 50 mL of deionized water. First 50 mmol of $NaHCO_3$ aqueous solution and then 15 mL of 2 M HCl was added to keep the pH at 9−10. Subsequently 50 mL of metal precursor solution, containing 5 mmol of $Ni(OAc)_2{\cdot}4H_2O$ and 20 mmol of $Mn(NO_3)_2{\cdot}4H_2O$, was added under vigorous stirring (note that the solution becomes immediately viscous, thus manual stirring is advisable). In the following step, the whole mixture was stirred at room temperature for 24 h, followed by filtration of the precipitate and washing with deionized water. The obtained solid was dried in vacuum at 80 °C overnight and then calcined at 500 °C for 4 h. Quantitative yield was observed.

Characterization. The solids were characterized by means of X-ray diffraction (XRD), nitrogen adsorption according to Brunauer−Emmett−Teller (BET), inductively coupled plasma optical emission spectroscopy (ICP-OES), transmission electron microscopy (TEM), and temperature-programmed-reduction (TPR). XRD was performed using a Bruker D8 Advance X-ray diffractometer with Cu $K_{\alpha 1}$ = 1.5418 Å radiation between 2° and 90° (2θ). Nitrogen sorption isotherms were measured at liquid-nitrogen temperature (−196 °C) with an Autosorb-1. The samples were degassed at 150 °C overnight before the measurement. The BET surface area was calculated by multiple-point (five-point) measurement. The mass content of Ni was measured by ICP-OES, using an ICP-OES 517 (Varian Inc., U.S.A.). TEM images were obtained on a Philips CM 12 instrument (120 keV), using carbon-coated copper grids. The specimens were dispersed in water with ultrasonication and loaded onto copper grids. TPR was performed in a fixed-bed silica reactor, similar to the reactor used in reaction, using 65 mg of catalyst diluted in a total volume of 1.25 mL of silica grains (Merck). The reactor was heated by an electric furnace (HTM Reetz). A gas mixture of 10% hydrogen in nitrogen (both Air Liquide) with a flow of 60 mL min^{-1} was used to reduce the samples. The concentration of hydrogen was detected via thermal conductivity detector (TCD, Messkonzept). The temperature was increased from room temperature to 750 °C with a heat ramp of 1 K min^{-1} and was held for 30 min. Hydrogen concentration and inner reactor temperature were logged in intervals of 5 seconds.

Catalytic Testing. The catalytic testing was performed in a fixed-bed reactor made of silica with an inner diameter of 5 mm and a length of 40 mm. Silica is known to have no catalytic activity on the reaction in the examined temperature range of 400−850 °C. The reactor was heated by an electric furnace (HTM Reetz). The catalyst bed consisted of varying masses of catalyst and silica grains (Merck) with a total volume of 1.25 mL. Before experiments started, the catalysts were in situ reduced in a pure hydrogen flow of 15 mL min^{-1} at a temperature of 500 °C for 1 h. Accordingly, the gas composition was chosen to be CH_4:CO_2:N_2 = 2:2:1 for both, screening and long-term experiments. Thereby, nitrogen was taken as internal standard for the gas analysis. Samples were taken after 25 min steady-state at each temperature point. Process gas analysis was performed by gas chromatography (HP 5890 Series II) equipped with methanizer, TCD, FID and mole sieve 5 Å and Hayesep Q columns (both Supelco). Argon was used to be carrier gas to detect small amounts of hydrogen in the process gas.

RESULTS AND DISCUSSION

In this study, two ternary oxide catalysts, bulk $Ni_{0.2}Mn_{0.8}O\_cp$ and supported $Ni_{0.2}Mn_{0.8}O\_cp\text{-}SiO_2$ were prepared using either a conventional co-precipitation method or a combination of co-precipitation and sol−gel process. For the bulk material the metal salts were dissolved and precipitated in basic conditions. In contrast, for supported ternary metal oxides, first a sodium silicate solution was prepared at controlled pH value. Addition of the metal salt solution yielded fast gelation of the silica precursor which was proven by the immediate increase in viscosity. Precipitation of the metal hydroxides occurs simultaneously or shortly after gelation of the silica yielding supported metal oxide precursors on a silica gel. Both obtained solids were then treated likewise, thus first calcined in ambient atmosphere at 500 °C for 4 h and then subjected to a reducing atmosphere (10% H_2 in Ar) at 500 °C for 1 h. PXRD measurements of the samples after calcination but before the reduction step (Supporting Information, Figure S1) indicate that a two phase mixture of $NiMnO_3$ and MnO_2 has formed for both the supported and unsupported sample. Aggregated nanoparticles of these oxides are observed which in the second case are supported on an amorphous porous silica (Supporting Information, Figure S2,3). H_2 TPR profiles (Supporting Information, Figure S4) of the as-made materials show two dominant peaks in temperature ranges between 200 and 250 °C and 300−350 °C, respectively, which can be attributed to the reduction sequence $MnO_2 \rightarrow Mn_3O_4 \rightarrow MnO$.

The PXRD patterns of the samples after reduction are presented in Figure 1, indicating that a solid solution of $Ni_xMn_{1-x}O$[34] has formed in both cases. A metal ratio

dx.doi.org/10.1021/cs3003963 | ACS Catal. 2013, 3, 224−229

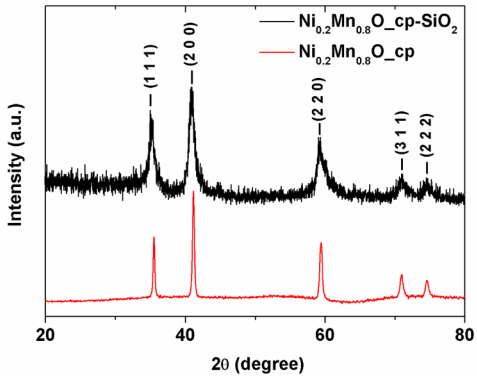

Figure 1. XRD patterns of $Ni_{0.2}Mn_{0.8}O$_cp and $Ni_{0.2}Mn_{0.8}O$_cp-SiO_2.

corresponding to $x = 0.2$ reflects the initial molar ratio of the metals used in the synthesis. This ratio was also found in the final oxide by ICP measurements (see Table 1). The similar peak positions in both patterns furthermore show that the simultaneous formation of an amorphous silica phase in $Ni_{0.2}Mn_{0.8}O$_cp-SiO_2 did not influence the crystal structure formation or composition of the ternary oxide. However, compared to $Ni_{0.2}Mn_{0.8}O$_cp, the pattern of $Ni_{0.2}Mn_{0.8}O$_cp-SiO_2 showed much broader and less intense peaks indicating the formation of smaller crystallites and the presence of the amorphous silica phase. Applying the Scherrer formula, an average crystallite size of around 30 nm is found for the bulk oxides, while this is largely reduced to around 10 nm for the supported oxides (Table 1). Also an increased surface area of 311 $m^2\ g^{-1}$ is found for $Ni_{0.2}Mn_{0.8}O$_cp-SiO_2 by nitrogen sorption measurements, owing to the smaller particle size of the metal oxide, but mainly because of the presence of a porous silica phase.

To further investigate the structure of the materials, TEM images of $Ni_{0.2}Mn_{0.8}O$_cp and $Ni_{0.2}Mn_{0.8}O$_cp-SiO_2 after reduction were obtained (Figure 2). Figure 2A and B show the sample $Ni_{0.2}Mn_{0.8}O$_cp obtained from co-precipitation. Large spherical aggregates in the range of 1.5−3 μm are observed, which are composed of smaller metal oxide particles with a size of approximately 100 nm, however with a broad size distribution. In contrast, for $Ni_{0.2}Mn_{0.8}O$_cp-SiO_2 (Figure 2C, D) no large metal oxide aggregates can be seen. Instead, metal oxide nanoparticles with a diameter of 6−10 nm are observed, which are dispersed on the amorphous silica support. The addition of the silica phase indeed efficiently suppressed the agglomeration and improved the dispersion of metal oxide nanoparticles. The here shown approach therefore provides a simple and feasible pathway for the one pot synthesis of supported metal oxide nanoparticles, even with mixed metal compositions.

$Ni_{0.2}Mn_{0.8}O$_cp and $Ni_{0.2}Mn_{0.8}O$_cp-SiO_2 were applied as catalysts for the DRM reaction. First it had to be verified if a ternary metal oxide of the here chosen composition, $Ni_{0.2}Mn_{0.8}O$, shows any catalytic activity for this reaction. Second we wanted to test, if and how the structure variation introduced by the here discussed one-pot approach influenced the catalyst performance.

Figure 3 shows the methane conversion as function of time on stream over both catalysts at a temperature of 525 °C. To compare the supported and the unsupported catalyst, the molar amount of nickel was kept constant. The reaction is controlled by its thermodynamics, leading to a maximum conversion of X_{eq} = 37% at 525 °C. Both catalysts, bulk and supported oxides, showed significant activity. Although, high GHSVs are chosen to avoid the occurrence of thermodynamic equilibrium, the more active $Ni_{0.2}Mn_{0.8}O$_cp-SiO_2 can easily achieve equilibrium conversion under these mild condition in the DRM reaction, which prevails over other reported Ni catalysts.[22−25] Moreover, $Ni_{0.2}Mn_{0.8}O$_cp-SiO_2 shows a much higher activity than $Ni_{0.2}Mn_{0.8}O$_cp among the whole course of the experiment. However, also a more significant deactivation is observed for the supported catalyst.

Elemental analysis was operated to investigate carbon deposition on the surface of the catalyst during the reaction, which could be one reason for the catalyst deactivation. Indeed after 40 h reaction at 525 °C, for both catalysts carbon deposition on the surface could be found.

To identify further changes in the structure of the catalyst, which could explain deactivation, XRD measurements were carried out on the material after 40 h DRM reaction at 525 °C (Figure 4).

In case of $Ni_{0.2}Mn_{0.8}O$_cp no considerable change in the XRD patterns is observed, beside a further increase in crystallite size (as shown in Table 1), indicating particle ripening or sintering during the DRM reaction, a possible reason for the observed slow deactivation. $Ni_{0.2}Mn_{0.8}O$_cp-SiO_2 also showed some enlargement of the $Ni_xMn_{1-x}O$ crystals, but additionally new distinct diffraction peaks attributed to formation of Ni^0 metal are observed. Accordingly the peaks corresponding to the metal oxide slightly shift to lower angles, which is due to the depletion of nickel in the solid solution.

Notably, the formation of small $Ni_xMn_{1-x}O$ nanoparticles seem to facilitate the diffusion of Ni species to the surface and thus the reduction of Ni^{2+} to metallic Ni^0, which is the main reason for the significantly enhanced activity of the supported solid solution, $Ni_{0.2}Mn_{0.8}O$_cp-SiO_2, as it is believed that reduced Ni^0 is the active site for the DRM reaction. Further growth or agglomeration of the first formed Ni^0 clusters, together with enhanced carbon deposition, is probably the reason for the stronger deactivation of the nanoparticulate catalyst with time.

Table 1. Summary of the Structural Properties of the Catalysts

			crystal size[b] (nm)		ICP	C deposition
name	method[a]	S_{BET} (m^2/g)	B.R.[c]	A.R.[d]	Ni_{mol}%[e]	wt %[f]
$Ni_{0.2}Mn_{0.8}O$_cp	cp	140	24.5/33.2	35.0/35.6	0.201	2.38
$Ni_{0.2}Mn_{0.8}O$_cp-SiO_2	cp-SiO_2	311	10.5/8.5	21.2/19.2	0.200	3.54/0.21

[a]cp: co-precipitation; cp-SiO_2: co-precipitation combined with a sol−gel process of $Na_2SiO_3{\cdot}5H_2O$. [b]The crystal size is derived from the Scherrer equation using the (1 1 1) and (2 0 0) peaks of the diffractogram. [c]B.R.: before the catalytic reaction. [d]A.R.: after 40 h at 525 °C in the DRM reaction. [e]Molar fraction of Ni/(Mn+Ni). [f]The results of carbon deposition was obtained by elemental analysis. $Ni_{0.2}Mn_{0.8}O$_cp was tested after the reaction at 525 °C for 40 h; $Ni_{0.2}Mn_{0.8}O$_cp-SiO_2 was tested after the reaction at 525 °C for 40 h and at 500 °C for 60 h, separately.

dx.doi.org/10.1021/cs3003963 | ACS Catal. 2013, 3, 224−229

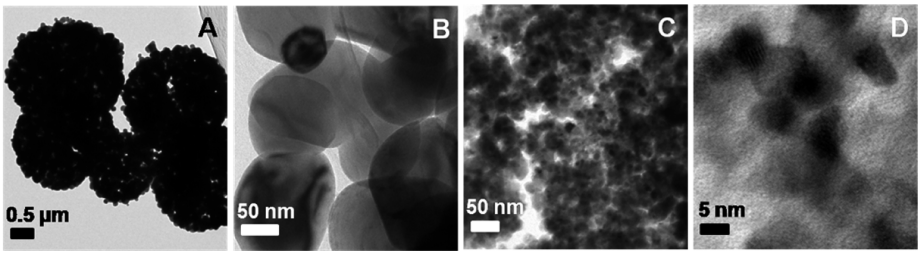

Figure 2. TEM images of $Ni_{0.2}Mn_{0.8}O$_cp (A, B) and $Ni_{0.2}Mn_{0.8}O$_cp-SiO_2 (C, D).

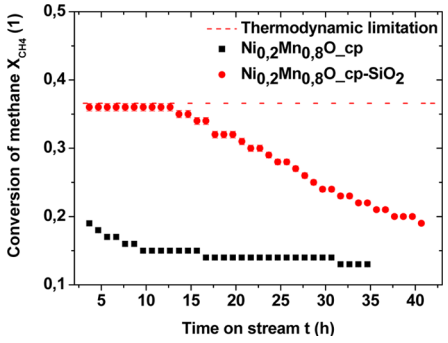

Figure 3. CH_4 conversion as a function of time on stream over catalysts $Ni_{0.2}Mn_{0.8}O$_cp and $Ni_{0.2}Mn_{0.8}O$_cp-SiO_2. Reaction temperature 525 °C, CH_4:CO_2:N_2:He = 1:1:0.5:7.5 (Note that a double amount of $Ni_{0.2}Mn_{0.8}O$_cp-SiO_2 was used to observe the same molar amount of Ni in both catalysts. For $Ni_{0.2}Mn_{0.8}O$_cp, m_{cat} = 50 mg, GHSV = 80 L h^{-1} g_{cat}^{-1}; for $Ni_{0.2}Mn_{0.8}O$_cp-SiO_2, m_{cat} = 100 mg, GHSV = 40 L h^{-1} g_{cat}^{-1}).

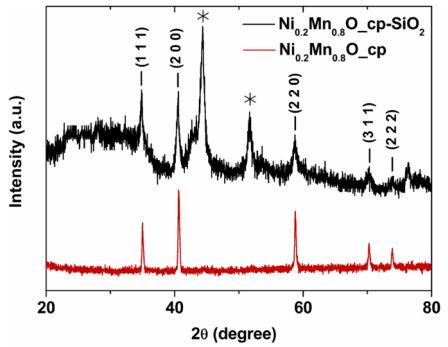

Figure 4. XRD patterns of $Ni_{0.2}Mn_{0.8}O$_cp and $Ni_{0.2}Mn_{0.8}O$_cp-SiO_2 after 40 h long-term measurement at a reaction temperature of 525 °C. The symbol denoted diffraction peaks of (*) – Ni^0 phase.

To obtain dynamic information about the formation of Ni^0 clusters or nanoparticles, PXRD patterns of the catalyst $Ni_{0.2}Mn_{0.8}O$_cp-SiO_2, after 1 h, 10 h, and 40 h DRM reaction were conducted (Figure 5). After 1 h reaction just very weak peaks for Ni^0 can be identified, while after 10 h these peaks become more noticeable, and finally become the most prominent feature in the diffractogram after 40 h reaction. Besides the relative intensity, the average size of the Ni^0 crystallites also increased with prolonged reaction time. Thus indeed the agglomeration of metallic Ni^0 clusters to larger Ni^0 nanoparticles can be seen as the main reason for the catalyst deactivation.

To verify the effect of the reaction temperature on the formation of Ni^0 and with this the stability of the supported solid solution catalyst, a long-time measurement using

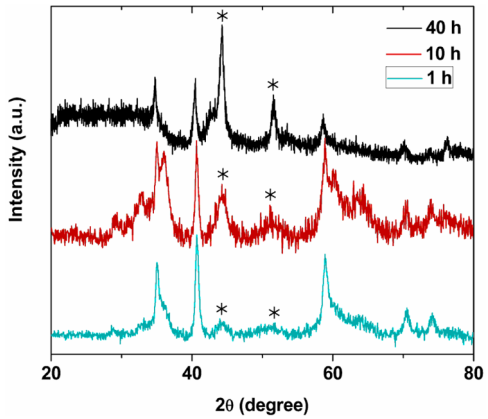

Figure 5. XRD patterns of $Ni_{0.2}Mn_{0.8}O$_cp-SiO_2 after 1 h, 10 h, and 40 h DRM reaction at a reaction temperature of 525 °C. The symbol denoted diffraction peaks of (*) – Ni^0 phase.

$Ni_{0.2}Mn_{0.8}O$_cp-SiO_2 was performed at 500 °C, 525 °C, and 550 °C, respectively (Figure 6).

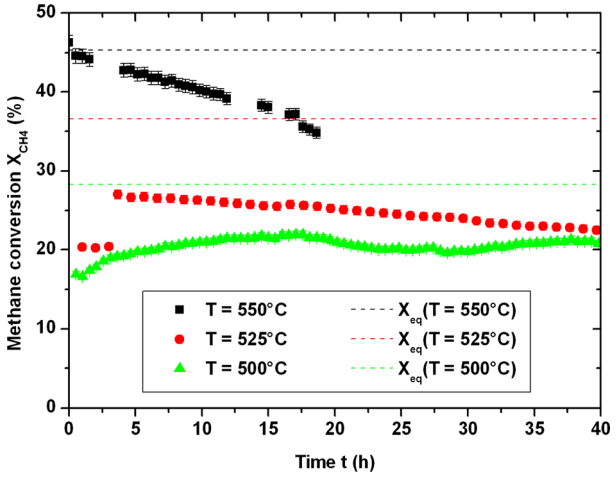

Figure 6. Long-term stability of $Ni_{0.2}Mn_{0.8}O$_cp-SiO_2 in DRM reaction. CH_4 conversion as a function of time on stream. (m_{cat} = 100 mg, CH_4:CO_2:N_2:He = 1:1:0.5:7.5, GHSV = 80 L h^{-1} g^{-1}.).

As expected, at 550 °C, the catalyst is deactivating rather fast. Because of the higher GHSV, the deactivation is observable from the beginning. The conversion shows no plateau at the thermodynamic limit as it was observed in Figure 3. Beside the formation of large Ni^0 nanoparticles, BET measurements revealed that the surface area of $Ni_{0.2}Mn_{0.8}O$_cp-SiO_2 decreased from 311 m^2 g^{-1} to 128 m^2 g^{-1} at 550 °C after 65 h reaction (GHSV of 40 L h^{-1} g^{-1}). Because of the non-ordered, amorphous nature of the support, no further

dx.doi.org/10.1021/cs3003963 | ACS Catal. 2013, 3, 224–229

information on changes of the porous characteristics of the support can be derived from TEM and nitrogen sorption isotherms before and after catalysis (Supporting Information, Figures S5–S8). However the significant decrease in surface area for the catalyst at 550 °C point to structural changes of the support, which can be an additional reason for the observed deactivation.

At 525 °C, the catalyst shows a lower rate of deactivation as for 550 °C. The first three points are measured at a temperature of 500 °C and reveal no trend of deactivation. Heating up to 525 °C, the conversion starts decreasing linearly and, after 40 h time on stream, it attains conversion for a temperature of 500 °C.

At 500 °C, the catalyst showed remarkable stability during the whole course of the reaction even after 40 h. Indeed PXRD of the catalyst after long-term measurement (Figure 7) with a

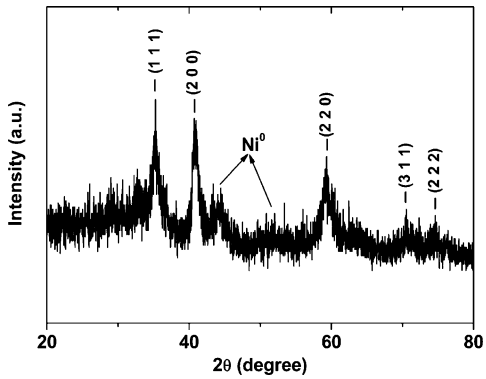

Figure 7. XRD patterns of $Ni_{0.2}Mn_{0.8}O$_cp-SiO_2 after 60 h long-term stability measurement at 500 °C.

GHSV of 40 L h^{-1} g^{-1} verified the assumption that no larger Ni^0 nanoparticles are formed at this temperature, instead, just very weak and broad peaks which can be attributed to the formation of Ni^0 are observed. Additionally the catalyst was investigated by elemental analysis. After a time on stream of 60 h at 500 °C with an equilibrium conversion of 28%, only a trace amount of carbon was observed (0.21%). One could conclude that at relative low temperature, the agglomeration of small Ni^0 clusters to larger particles can be avoided and therefore also the formation of carbon deposition was suppressed, which ensured the stability of the catalyst.

CONCLUSION

A ternary metal oxide catalyst $Ni_{0.2}Mn_{0.8}O$ dispersed on porous silica was prepared using a one-pot co-precipitation/sol–gel process. Compared to bulk $Ni_{0.2}Mn_{0.8}O$ prepared by a conventional co-precipitation method, the silica supported $Ni_{0.2}Mn_{0.8}O$ catalyst is composed of much smaller metal oxide crystallites with the size of 8–10 nm yielding significant enhancement in activity in the DRM reaction. Indeed the material showed significant activity for low temperature DRM reaction (below 550 °C), which prevails over other reported Ni catalyst in the DRM reaction, and the thermodynamic equilibrium could be achieved under very mild conditions. The easier formation of small metallic Ni-clusters seem to be the main reason of the significant activity increase of $Ni_{0.2}Mn_{0.8}O$ nanoparticles supported on SiO_2 in comparison to the bulk. However, the formation of such small clusters yields fast agglomeration to larger Ni^0 nanoparticles, especially at higher temperatures. Therefore catalyst deactivation is observed at 525 and 550 °C accompanied by carbon deposition. However, the formation of large Ni(0) nanoparticles is not observed at 500 °C and at this temperature, the supported catalyst $Ni_{0.2}Mn_{0.8}O$ was remarkably stable with high activity even after 40 h reaction.

ASSOCIATED CONTENT

Supporting Information

XRD, TEM, and H2 TPR measurements of the materials before reduction, TEM, N_2 sorption measurements after catalysis. This material is available free of charge via the Internet at http://pubs.acs.org.

AUTHOR INFORMATION

Corresponding Author

*E-mail: arne.thomas@tu-berlin.de (A.T.), schomaecker@tu-berlin.de (R.S.).

Author Contributions

‖Both authors contributed equally to this paper.

Notes

The authors declare no competing financial interest.

ACKNOWLEDGMENTS

This work is funded by Unifying Concepts in Catalysis (UniCat). The authors acknowledge Dr. Caren Göbel for TEM measurements, Mrs. Christina Eichenauer for BET measurements, and Ms. Maria Unterweger for XRD measurements. Dr. Sabine Wrabetz from the Fritz Haber Institute of the MPG in Berlin is acknowledged for her help during mechanistic studies.

REFERENCES

(1) Liu, C.; Ye, J.; Jiang, J.; Pan, Y. *ChemCatChem* **2011**, *3*, 529–541.
(2) York, A. P. E.; Xiao, T.; Green, M. L. H.; Claridge, J. B. *Catal. Rev.* **2007**, *49*, 511–560.
(3) Araujo, G. C. de; Lima, S. M. de; Assaf, J. M.; Peña, M. A.; Fierro, J. L. G.; do Carmo Rangel, M. *Catal. Today* **2008**, *133–135*, 129–135.
(4) Choudhary, V.; Mondal, K. *Appl. Energy* **2006**, *83*, 1024–1032.
(5) Pichas, C.; Pomonis, P.; Petrakis, D.; Ladavos, A. *Appl. Catal., A* **2010**, *386*, 116–123.
(6) Vella, L. D.; Villoria, J. A.; Specchia, S.; Mota, N.; Fierro, J. L. G.; Specchia, V. *Catal. Today* **2011**, *171*, 84–96.
(7) Peters, A.; Nouroozi, F.; Richter, D.; Lutecki, M.; Glaeser, R. *ChemCatChem* **2011**, *3*, 598–606.
(8) Özkara-Aydınoğlu, Ş.; Aksoylu, A. E. *Int. J. Hydrogen Energy* **2011**, *36*, 2950–2959.
(9) Zhang, S.; Wang, J.; Liu, H.; Wang, X. *Catal. Commun.* **2008**, *9*, 995–1000.
(10) Wang, S. *Appl. Catal., B* **1998**, *16*, 269–277.
(11) Gaur, S.; Haynes, D. J.; Spivey, J. J. *Appl. Catal., A* **2011**, *403*, 142–151.
(12) Sarusi, I.; Fodor, K.; Baán, K.; Oszkó, A.; Pótári, G.; Erdohelyi, A. *Catal. Today* **2011**, *171*, 132–139.
(13) Zeppieri, M.; Villa, P. L.; Verdone, N.; Scarsella, M.; Filippis, P. D. *Appl. Catal., A* **2010**, *387*, 147–154.
(14) Coronel, L.; Múnera, J. F.; Lombardo, E. A.; Cornaglia, L. M. *Appl. Catal., A* **2011**, *400*, 185–194.
(15) Sadykov, V. A.; Gubanova, E. L.; Sazonova, N. N.; Pokrovskaya, S. A.; Chumakova, N. A.; Mezentseva, N. V.; Bobin, A. S.; Gulyaev, R. V.; Ishchenko, A. V.; Krieger, T. A.; Mirodatos, C. *Catal. Today* **2011**, *171*, 140–149.
(16) Pieterse, J. A. Z.; Boon, J.; van Delft, Y. C.; Dijkstra, J. W.; van Den Brink, R. W. *Catal. Today* **2010**, *156*, 153–164.

(17) Yamazaki, O.; Nozaki, T.; Omata, K.; Fujimoto, K. *Chem. Lett.* **1992**, *21*, 1953−1954.
(18) Yamazaki, O.; Tomishige, K.; Fujimoto, K. *Appl. Catal., A* **1996**, *136*, 49−56.
(19) Chen, Y.; Yamazaki, O.; Tomishige, K.; Fujimoto, K. *Catal. Lett.* **1996**, *39*, 91−95.
(20) Bradford, M. C. J.; Vannice, M. A. *Appl. Catal., A* **1996**, *142*, 73−96.
(21) Hu, Y. H.; Ruckenstein, E. *Catal. Lett.* **1997**, *43*, 71−77.
(22) Chen, Y.; Tomishige, K.; Yokoyama, K.; Fujimoto, K. *Appl. Catal., A* **1997**, *165*, 335−347.
(23) Meshkani, F.; Rezaei, M. *Int. J. Hydrogen Energy* **2010**, *35*, 10295−10301.
(24) Sokolov, S.; Kondratenko, E. V.; Pohl, M.-M.; Barkschat, A.; Rodemerck, U. *Appl. Catal., B* **2012**, *113*−*114*, 19−30.
(25) Gonzalez-Delacruz, V. M.; Pereñiguez, R.; Ternero, F.; Holgado, J. P.; Caballero, A. *ACS Catal.* **2011**, *1*, 82−88.
(26) Hu, Y. H.; Ruckenstein, E. *Catal. Lett.* **1996**, *36*, 145−149.
(27) Hu, Y. H.; Ruckenstein, E. *Langmuir* **1997**, *13*, 2055−2058.
(28) Hu, Y. *J. Catal.* **1996**, *163*, 306−311.
(29) Christel, L.; Pierre, A.; Abel, D. A.-M. R. *Thermochim. Acta* **1997**, *306*, 51−59.
(30) Zhu, J.; Xie, X.; Carabineiro, S. A. C.; Tavares, P. B.; Figueiredo, J. L.; Schomäcker, R.; Thomas, A. *Energy Environ. Sci.* **2011**, *4*, 2020.
(31) Nowag, S.; Wang, X.-S.; Keilitz, J.; Thomas, A.; Haag, R. *ChemCatChem* **2010**, *2*, 807−811.
(32) Boualleg, M.; Basset, J.-M.; Candy, J.-P.; Delichere, P.; Pelzer, K.; Veyre, L.; Thieuleux, C. *Chem. Mater.* **2009**, *21*, 775−777.
(33) Song, H.; Rioux, R. M.; Hoefelmeyer, J. D.; Komor, R.; Niesz, K.; Grass, M.; Yang, P.; Somorjai, G. A. *J. Am. Chem. Soc.* **2006**, *128*, 3027−37.
(34) Barrett, C. A.; Evans, E. B. *J. Am. Ceram. Soc.* **1964**, *47*, 533−533.